Molecular Therapy
Nucleic Acids
Original Article

AMERICAN SOCIETY of GENE & CELL THERAPY

MicroRNA-672-5p Identified during Weaning Reverses Osteopenia and Sarcopenia in Ovariectomized Mice

Naseer Ahmad,[1] Priyanka Kushwaha,[1] Anirudha Karvande,[1] Ashish Kumar Tripathi,[1] Priyanka Kothari,[1] Sulekha Adhikary,[1] Vikram Khedgikar,[1] Vijay Kumar Mishra,[1] and Ritu Trivedi[1]

[1]Division of Endocrinology, CSIR-CDRI (Council of Scientific and Industrial Research-Central Drug Research Institute), Sector 10, Jankipuram Extension, Sitapur Road, Lucknow 226031, Uttar Pradesh, India

Post-menopausal condition augments the biological aging process, characterized by multiple metabolic disorders in which bone loss is the most prevalent outcome and usually coupled with sarcopenia. Coexistence of such associated pathogenesis have much worse health outcomes, compared to individuals with osteoporosis only. Pre- and post-natal bone development demands calcium from mother to fetus during pregnancy and lactation leading to a significant maternal skeletal loss. It follows an anabolic phase around weaning during which there is a notable recovery of the maternal skeleton. Here, we have studied the therapeutic effect of microRNA-672-5p identified during weaning when it is predominantly expressed, in ovariectomized mice for both osteopenia and sarcopenia. miR-672-5p induced osteoblast differentiation and mineralization. These actions were mediated through inhibition of Smurf1 with enhanced Runx2 transcriptional activation. *In vivo*, miR-672-5p significantly increased osteoblastogenesis and mineralization, thus reversing bone loss caused by ovariectomy. It also improved bone-mineral density, load-bearing capacity, and bone quality. Sarcopenia was also alleviated by miR-672-5p, as we observed increased cross-sectional area and Feret's diameter of muscle fibers. We hypothesize that elevated miR-672-5p expression has therapeutic efficacy in estrogen-deficiency-induced osteopenia along with sarcopenia.

INTRODUCTION

Diminution of bone and muscle with increasing age depicts a vast threat to loss of self-standing in later life.[1] Post-menopausal conditions expedite the biological aging process and represent multiple metabolic disorders.[2] However, the reduction in bone mass is the most important biological consequence after menopause and commonly accompanied with sarcopenia. Coexistence of such integrated pathogenesis has considerably worse health consequences than for the individuals with osteoporosis only. Some clinical studies from Italian and Korean populations reported that 58% high prevalence of hip fracture and significant low bone-mineral density (BMD) in individuals with sarcopenia, respectively, indicate a higher risk of fractures.[3,4] Interestingly, mechanical effect of muscle loading directly regulates bone strength.[5] Wasting of bone and muscle mass simultaneously, both in normal aging and pathological conditions, can lead to increased risk of fracture and immobility.[6] Loss of muscle mass can lead to poor balance and falls, and these falls are probably responsible to increase the chances of fractures due to the inability of bones to bear load in osteoporosis conditions.[6] Unfortunately, there is no current anti-osteoporotic drug that prevents menopause-associated loss of bone and muscle mass. Hence, an approach to concurrently attenuate menopause-associated bone and muscle loss would now be regarded as an exemplary molecular pharmacotherapy.

Currently, studies in therapeutic discovery have shown the notability of microRNAs (miRNAs) that control bone homeostasis and remodeling during normal and osteoporotic conditions.[7–9] miRNAs are now emerging to play an important role in skeletogenesis.[10] Particularly, the conditional deletion of the miRNA-processing Dicer in osteoblast lineage cells reveals a direct need of miRNAs in embryonic skeletogenesis, post-natal bone growth, modeling, as well as remodeling.[11] Small non-coding RNAs, also known as miRNAs, effectuate translational repression or degradation of a transcript by binding of miRNAs to complementary sequence sites of the target mRNAs. This allows successful control of gene expression over genomic interactions between transcription factors and their associated elements. Here, we investigate the role of miRNA-672-5p identified at the time of weaning, and that is an anabolic target to the skeleton.[12] Recently, we investigated miRNA expression during lactation and weaning, the two phases of reproduction distinguished by noticeable variations in bone formation and resorption.[12] There is an intense maternal bone loss during lactation to manage the requirement of calcium

Received 10 July 2018; accepted 3 January 2019;
https://doi.org/10.1016/j.omtn.2019.01.002.

Correspondence: Ritu Trivedi, Division of Endocrinology, CSIR-CDRI (Council of Scientific and Industrial Research-Central Drug Research Institute), Sector 10, Jankipuram Extension, Sitapur Road, Lucknow 226031, Uttar Pradesh, India.
E-mail: ritu_trivedi@cdri.res.in

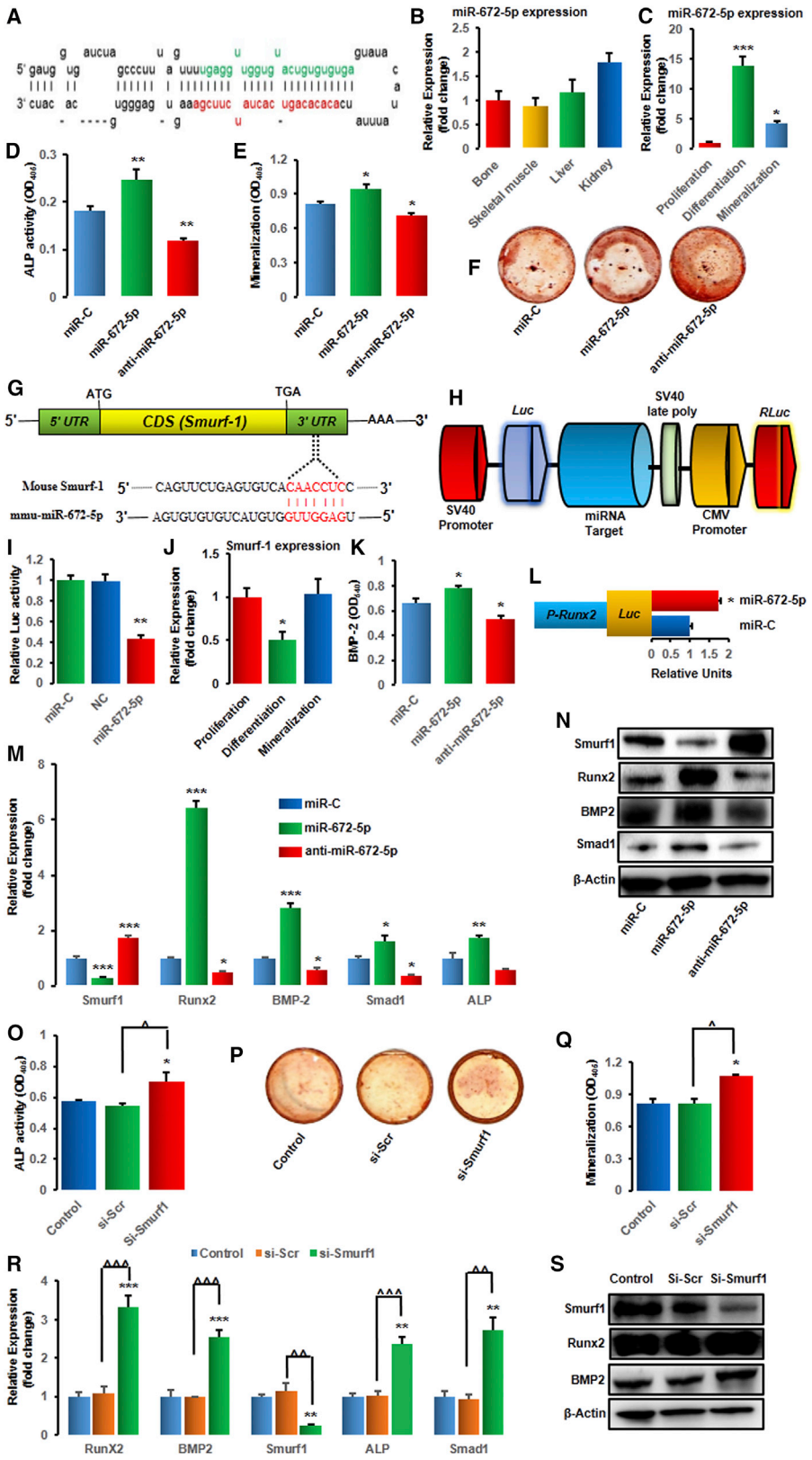

(legend on next page)

for post-natal skeletal growth and modeling. However, this bone loss is restored by the quick new bone formation that renews the maternal skeleton during weaning.[13] If these procedures begin to be uncoupled, then pregnancy- and lactation-related osteoporosis develops.[13] There is proof for interconnection between breastfeeding and fractures, strengthening the proposition that prolonged lactation may lead to a substantial risk of osteoporosis-associated fractures in post-menopausal women.[14] Corroborating the ability and distinctiveness of this quick remodeling phase, rodents, which usually suckle many offspring during lactation period of 21 days, can lose their bone-mineral content up to the level of 35%. This loss of bone is restored totally after weaning. Therefore, the weaning phase is regarded as the most anabolic phase in the reproductive window of a rodent and gives a vital window to identify new anabolic targets.[15–17]

Previously, we have identified eight miRNAs, and their expressions were modulated basically during weaning.[12] Further, we selected to investigate the role of miR-672-5p on the osteoblast both *in vitro* and *in vivo* as well as on ovariectomized (OVx)-induced sarcopenia. Ovariectomy represents a well-known model of post-menopausal-induced osteopenia where sarcopenia occurs concurrently,[18] hence mimicking the human post-menopausal situation. In this study, using the OVx mouse model, we studied the effect of miR-672-5p in restoring osteopenia and sarcopenia. Finally, we conclude that miR-672-5p encourages osteoblast differentiation, mineralization, and bone formation, attenuates OVx-induced sarcopenia, and, therefore, that it might not only intervene in skeletal recovery after weaning and OVx-induced sarcopenia, but also have wider implications as a potential target for conditions of menopause-induced loss of bone and muscle.

RESULTS

miR-672-5p Represses Smurf1 to Promote Osteoblast Differentiation

We had identified eight miRNAs in bone-marrow-derived osteoblasts whose expressions were differentially regulated between lactation and weaning.[12] Notably, out of a total 4,716 detected miRNAs, the expression of miR-672-5p, miR-874-3p, miR-327, miR-451, and miR-212 was increased, while the expression of miR-204, miR-322-3p and miR-664 was decreased during weaning.[12] Further, these miRNAs were validated by qPCR in osteoblasts derived from bone marrow cells BMCs and/or primary calvarial osteoblasts.[12] Significant increase in miR-672-5p (miRNA precursor stem-loop secondary structure; Figure 1A) during weaning (in osteoblasts derived from BMCs) and in calvarial osteoblasts,[12] with notable expression in bone, skeletal muscle, liver, and kidney (Figure 1B), suggested it to be an important target. Moreover, the expression of miR-672-5p enhanced significantly during osteoblast differentiation (~13.0 fold) and mineralization (~4.0-fold), compared with proliferation stage (Figure 1C).

Transfection with miR-672-5p mimic in osteoblasts enhanced their differentiation. Alkaline phosphatase (ALP) activity (Figure 1D) and mineralizing ability (Figure 1E) were enhanced significantly, consistent with the higher forms of a mineralized nodule of osteoblastic colony-forming units (Cfu-ob) (Figure 1F), whereas the miR-672-5p inhibitor (anti-miR-672-5p) significantly decreased ALP activity, mineralization, and Cfu-ob colonies (Figures 1D–1F).

We aimed to predict the mRNA target gene for miR-672-5p using TargetScan and miRBase. Smurf1 was found to be the putative target gene, which revealed a seven-nucleotide seed sequence match with miR-672 in the 3′ UTR (Figure 1G). Smurf1 inhibits osteoblast

Figure 1. miR-672-5p Represses Smurf1 to Promote Osteoblast Differentiation

(A) Stem-loop structure of miR-672 predicted by miR-base (the mature miR-672-5p sequence is shown in green). (B and C) Expression (qPCR, in triplicate) of miR-672-5p in different tissues (B) and cells, i.e., in osteoblasts during proliferation, differentiation, or mineralization (C). Data are mean ± SE. *$p < 0.05$ and ***$p < 0.001$ compared with proliferation stage of osteoblasts. (D–F) Effect of transfection of osteoblasts with the mimic (miR-672-5p), inhibitor (anti-miR-672-5p), and miR-C (control) on ALP (alkaline phosphatase) activity (OD, n = 8) (D) and mineralization (OD, n = 4) (E). (F) Representative wells showing alizarin-positive colony (Cfu-ob) formation in osteoblast cell cultures on day 15 in osteogenic medium. Data are mean ± SE. *$p < 0.05$ and **$p < 0.01$ compared with miR-C. (G) Identification of miR-672-5p target gene in osteoblasts and computational analysis was performed for the complementarities of miR-672-5p to the 3′ UTR of Smurf1 and (H) schematic presentation of the reporter plasmid used to illustrate the effect of Smurf1 3′ UTR on luciferase activity. CMV, cytomegalovirus promoter; Luc, luciferase; RLuc, renilla luciferase. (I) Effect of miR-672-5p overexpression on a dual luciferase reporter plasmid containing Smurf1 3′ UTR was analyzed. Cells were co-transfected with the WT-pEZX-MT06-Smurf1 or an empty vector (NC, negative control) and miR-672-5p or miR-C. Firefly and renilla luciferases were measured in the cell lysate. Data are mean ± SE of three independent measurements. **$p < 0.01$ compared with miR-C. (J) Expression (qPCR, in triplicate) of Smurf1 in osteoblasts during proliferation, differentiation, or mineralization. Data are mean ± SE. *$p < 0.05$ compared with proliferation stage of osteoblasts. (K) Transfection of osteoblasts with the mimic (miR-672-5p) enhanced the release of BMP2 in conditioned medium (BMP2 ELISA). Data are mean ± SE of three independent experiments. *$p < 0.05$ compared with miR-C. (L) Effect of miR-672-5p or scrambled miR-C on Runx2 promoter activity using a luciferase (Luc) reporter. Data are mean ± SE of three independent experiments. *$p < 0.05$ compared with miR-C. (M) qPCR (in triplicate) was performed for Smurf1 (a direct target gene of miR-672-5p) or the osteoblast differentiation genes, including Runx2, BMP2, Smad1, and ALP after 48 h of transfection. Data are mean ± SE. *$p < 0.05$, **$p < 0.01$, and ***$p < 0.001$ compared with miR-C. (N) Western blot analysis was done for Smurf1 (ab38866-Abcam; 1:1,000), Runx2 (ab76956-Abcam; 1:1000), BMP2 (ab14933-Abcam; 1:1000), and Smad1 (ab63356-Abcam; 1:1,000) after 48 h of transfection. β-actin (sc-47778 Santa Cruz Biotechnology; 1:500) was taken as a loading control. Secondary antibodies (either anti-rabbit or anti-mouse; 1:10,000) were horseradish peroxidase (HRP) conjugated (Sigma-Aldrich). (O–S) miR-672-5p represses Smurf1, which promotes the upregulation of Runx2 and osteoblast differentiation. (O) ALP activity (OD, n = 8), (P) Cfu-ob formation, (Q) mineralization (OD, n = 4), and (R) mRNA expression of Runx2, BMP2, Smurf1, ALP, and Smad1 (qPCR, in triplicate), and (S) protein expression of Smurf1 (ab38866-Abcam; 1:1,000), Runx2 (ab76956-Abcam; 1:1000), and BMP2 (ab14933-Abcam; 1:1,000) in either control osteoblasts or transfected with siRNA against Smurf1 or scrambled siRNA (Si-Scr). β-actin (sc-47778 Santa Cruz Biotechnology; 1:500) was taken as a loading control. Secondary antibodies (either anti-rabbit or anti-mouse; 1:10,000) were HRP conjugated (Sigma-Aldrich). Data are mean ± SE. *$p < 0.05$, **$p < 0.01$, and ***$p < 0.001$ compared with miR-C or control. Other comparisons, ^$p < 0.05$, ^^$p < 0.01$, and ^^^$p < 0.001$ as shown.

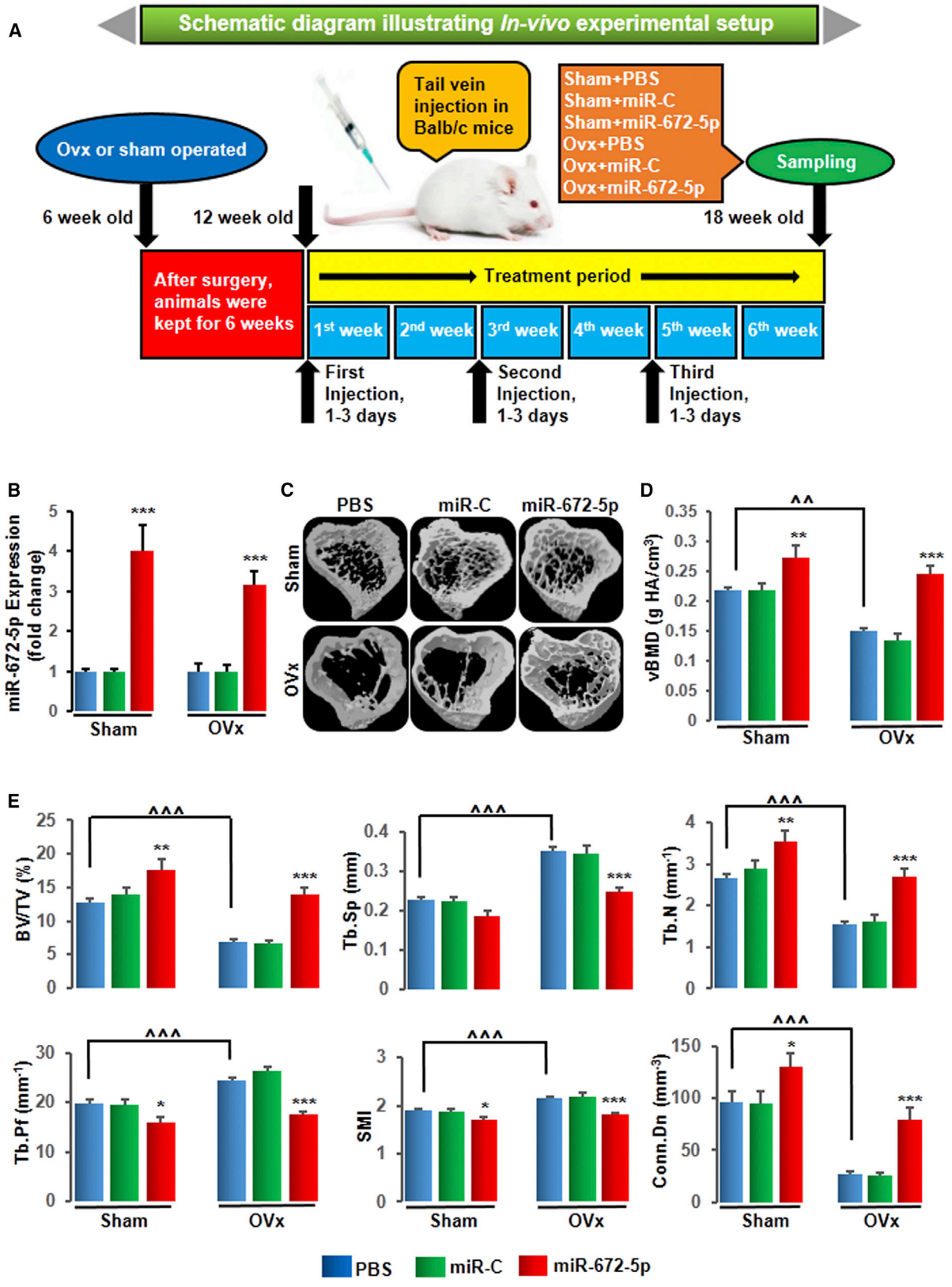

(legend on next page)

differentiation and bone formation *in vitro* and *in vivo*, and downregulation of Smurf1 increases bone formation.[19–21] To check whether miR-672-5p can directly target Smurf1, a luciferase reporter assay was done, which contained the wild-type 3′ UTR of Smurf1 (Figure 1H). In addition, a luciferase reporter construct (an empty plasmid vector) was also used as a negative control. The wild-type and negative control luciferase expression vectors were co-transfected with either mimic of miR-672-5p or miR-C in calvarial osteoblasts, and then levels of luciferase activity were estimated. Transfection of miR-672-5p mimic repressed the luciferase activity, confirming the specificity of the action (Figure 1I). Additionally, by qPCR analysis, we also checked the expression of Smurf1 during osteoblast differentiation, corroborating the data of miRNA-672-5p endogenous expression (Figure 1J).

In agreement with *in silico* information and luciferase data, we noticed that the mimic of miR-672-5p inhibited Smurf1 expression; in contrast, the inhibitor stimulated its expression in primary mouse calvarial osteoblast cells (Figure 1M), with confirmation at the protein level (Figure 1N). On one hand, with mimic, qPCR analysis disclosed increased expression of osteogenic genes, including Runx2, BMP2, Smad1, and ALP in osteoblasts; on the other hand, these effects were reversed with the inhibitor (Figure 1M). Taken together, data suggests that miR-672-5p stimulates osteoblast differentiation and mineralization.

To examine this process, co-transfection of the Runx2 promoter (pRunx2-Luc) (catalog no. MPRM13038, GeneCopoeia) was done, and the mimic of miR-672-5p promoted Runx2 promoter activity (Figure 1L) that revealed that miR-672-5p promoted osteoblast differentiation by directly targeting Smurf1 and indirectly protecting Runx2. In addition, the levels of BMP2 (in conditioned media) was increased with mimic and reversed with inhibitor (Figure 1K).

We subsequently investigated whether Smurf1 suppression was necessary for miR-672-5p-induced Runx2 activation throughout osteoblast differentiation. Silencing of Smurf1 with small interfering RNA (siRNA) in osteoblasts enhanced ALP activity (Figure 1O), Cfu-ob formation (Figure 1P), and mineralization (Figure 1Q) when compared with scrambled siRNA. Moreover, we evaluated the expression of Runx2 and its target genes including BMP2, Smad1, and ALP, in Smurf1-deprived cells, which showed a remarkably enhanced expression of Runx2 and its target genes at the mRNA levels (Figure 1R). In addition, Smurf1, Runx2, and BMP2 expressions at protein level were also confirmed (Figure 1S). Data from the knockdown study indicate that Smurf1 downregulation was required for miR-672-5p-induced Runx2 activation in osteoblast differentiation (Figures 1R and 1S).

In Vivo Validation of miR-672-5p Restores Ovariectomy-Induced Bone Loss and Biomechanical Properties

To study the anabolic response of miR-672-5p *in vivo* system, we administered the mimic of miR-672-5p (7.0 mg/kg) or scrambled miRNA (7.0 mg/kg) or PBS (0.2 mL, as vehicle) intravenously through tail vein in OVx or sham-operated mice for 6 weeks on days 1–3 of the first, third, and fifth weeks (Figure 2A).[12] We first estimated the expression of miR-672-5p in bone tissues to show successful *in vivo* tissue delivery and uptake in OVx and sham-operated mice (Figure 2B). We next assessed trabecular bone at three sites, including femoral and tibial metaphyses and the vertebral column. Representative 3D images of femoral (Figure S1A) and tibial (Figure 2C) metaphyses were generated by micro-computed tomography (μ-CT). We noticed that OVx mice showed decreased volumetric BMD (vBMD) at all three sites including femur (by ∼24%) (Figure S1B), tibia (by ∼36%) (Figure 2D), and the vertebral column (by ∼22%) (Table 1) compared with corresponding sham-PBS mice. As believed, OVx mice showed decreased bone volume to tissue volume (BV/TV), trabecular number (Tb.N), and connection density (Conn.Dn) and increased trabecular separation (Tb.Sp), trabecular pattern factor (Tb.Pf), and structure model index (SMI) at femoral (Figure S1C) and tibial (Figure 2E) sites. Compared with corresponding sham-PBS mice, the significant loss of trabecular bone in femur (BV/TV by ∼34%) and tibia (BV/TV by ∼45%) in OVx mice was moderately restored (femur, BV/TV by ∼62%; and tibia, BV/TV by ∼101%) by the miR-672-5p mimic; in contrast, miR-C and vehicle were both inefficacious (Figure S1C and Figure 2E). Next, we assessed trabecular bone of vertebra column and found the same results as in the case of femur and tibia except for Tb.Sp (Table 1). In addition, we observed that the mimic enhanced femoral bone mechanical parameters, including power (by ∼83%), strength (by ∼155%), and stiffness (by ∼40%) (Figure S1D), not only in OVx but also in sham-operated mice. Vertebral column mechanical strength (by ∼44%) and stiffness (by ∼40%) (Table 1) were also increased by mimic in OVx mice.

miR-672-5p Treatment Has an Anabolic Effect and Promotes Bone Formation

On one hand, immunohistochemistry data showed that the expression of the Smurf1 protein was increased in the bone of OVx mice and reversed by the mimic treatment by increasing the expression of the Runx2 protein (Figure 3A). GT (Goldner's trichrome) staining

Figure 2. miR-672-5p Treatment Restores Ovariectomy-Induced Trabecular Bone Loss in Tibia Bones

(A) Schematic diagram illustrating *in vivo* experimental setup. (B) Enhanced miR-672-5p expression (qPCR, in triplicate) in bone following injection of a mimic of miR-672-5p using Invivofectamine 3.0 reagent into 12-week-old female BALB/c mice at the end of 6 weeks of treatment, and this indicates sufficient tissue uptake. Data are mean ± SE. ***$p < 0.001$ compared with the PBS-treated group. (C) Representative 3D images of the tibia bones generated by micro-CT. (D) Volumetric bone-mineral density (vBMD) in the tibia at the end of 6 weeks of treatment was improved. Data are mean ± SE. **$p < 0.01$ and ***$p < 0.001$ compared with the PBS-treated group, or as shown ^^$p < 0.01$; $n \geq 6$ mice per group. (E) Structural micro-CT parameters for trabecular bone, including BV/TV, Tb.Sp, Tb.N, Tb.Pf, SMI, and Conn.Dn (units are shown) in the tibia epiphyses. Data are mean ± SE. *$p < 0.05$, **$p < 0.01$, and ***$p < 0.001$ compared with the PBS-treated group, or as shown ^^^$p < 0.001$; $n = 8$ mice per group. See also Figure S1 and Table 1 for femur and vertebrae, respectively.

Table 1. miR-672-5p Improves micro-CT Parameters and Biomechanical Properties in Vertebra of Mice

Parameters	PBS	miR-C	miR-672-5p	PBS	miR-C	miR-672-5p
	Sham			**OVx**		
vBMD (gHA/cm^3)	0.317 ± 0.007	0.299 ± 0.011	0.358 ± 0.036	0.247 ± 0.031 (ns)	0.239 ± 0.028	0.347 ± 0.014[a]
BV/TV (%)	21.62 ± 0.44	21.17 ± 0.54	24.93 ± 0.3.11	15.36 ± 0.99[c]	16.45 ± 0.61	22.17 ± 0.81[a]
Tb.N (mm^{-1})	4.22 ± 0.12	4.48 ± 0.20	4.57 ± 0.39	3.08 ± 0.32[c]	3.16 ± 0.21	4.13 ± 0.12[a]
Tb.Pf (mm^{-1})	7.08 ± 0.49	6.96 ± 1.03	6.82 ± 0.83	11.10 ± 1.01[d]	10.51 ± 1.02	6.22 ± 0.37[b]
SMI	1.133 ± 0.045	1.135 ± 0.044	0.985 ± 0.056	1.417 ± 0.057[c]	1.361 ± 0.079	1.154 ± 0.058[b]
Conn.Dn (1/mm^3)	186.8 ± 15.46	205.2 ± 18.22	219.6 ± 19.28	105.9 ± 18.33[d]	97.4 ± 12.01	161.7 ± 14.0[a]
Strength (mJ)	213.7 ± 15.33	215.5 ± 11.60	261.7 ± 17.68	144.4 ± 15.04[c]	160.6 ± 17.66	208.7 ± 7.38[a]
Stiffness (N/mm)	696.6 ± 27.05	676.2 ± 28.98	788.9 ± 86.50	443.0 ± 30.54[d]	476.8 ± 33.26	620.7 ± 35.48[a]

miR-672-5p treatment restores bone loss and biomechanical properties in the vertebral bone of OVx mice at the end of 6 weeks of treatment. Table 1 shows volumetric bone-mineral density (vBMD), structural micro-CT parameters for trabecular bone, including bone volume to tissue volume (BV/TV), trabecular number (Tb.N), trabecular pattern factor (Tb.Pf), structure model index (SMI) and connection density (Conn.Dn), and bone biomechanical parameters like strength and stiffness (units are shown). Data are mean ± SE. ns, statistically non-significant; n = 6 mice per group. See also Figures 2 and S1.
[a]$p < 0.05$ and [b]$p < 0.01$ compared with the OVx-PBS-treated group or [c]$p < 0.05$ and [d]$p < 0.01$compared with the Sham-PBS-treated group.

representative images (Figure 3B) and data showed significant enhancement in bone surface density (BS/TV) with miR-672-5p treatment (Figure 3C). On the other hand, because miR-672-5p enhanced osteoblast differentiation *in vitro*, we assessed serum P1NP, an established osteogenic agent. OVx mice showed a significant decrease in P1NP compared with sham-operated animals, and miR-672-5p increased it to sham levels (Figure 3D). These noticeable anabolic functions were also proved by an intense effect on indices of bone formation (calcein double-labeling representative images; Figure 3E); specifically, significant enhancement in mineralizing surface per bone surface (MS/BS), mineral apposition rate (MAR), and bone formation rate/bone surface (BFR/BS) (Figure 3F). In addition, OVx mice resulted in bone resorption, as shown by the high number of osteoclasts per bone surface (Oc.N/BS) and the greater percentage of surfaces covered by osteoclasts (Oc.S/BS) than sham-operated mice[22] (Figures S2A–S2C). OVx mice treated with miR-672-5p did not affect the Oc.N/BS and Oc.S/BS compared to either OVx-PBS or OVx-miR-C treated mice (Figures S2A–S2C), and this data is consistent with previous reports that alteration of smurf1 does not affect osteoclast function.[19,20,23]

miR-672-5p Treatment Represses Smurf1 *In Vivo* to Promote Osteoblastogenesis

To investigate the mechanism of the accruement in bone mass at cellular levels by miR-672-5p, we flushed out BMCs in osteoblast differentiation medium after 6 weeks of treatment. In *ex vivo* culture, OVx mice showed a depletion in ALP activity (Figure 4A), mineralization (Figure 4B), and formation of Cfu-ob (Figure 4C), accordant with low-turnover loss of bone. However, neither miR-C nor vehicle influence these *ex vivo* parameters, but the mimic relatively increased ALP activity, mineralization, and formation of Cfu-ob (Figures 4A–4C). Moreover, consistent with *in vitro* transfection data (Figure 1), the expression of Runx2 and BMP2 was enhanced (and Smurf1 suppressed) in bone tissues at mRNA (Figures 4D–4F) and protein (Figure 4G) level from miRNA-672-5p mimic-treated mice compared with miR-C or PBS-vehicle-treated mice. These data demonstrate that the *in vivo* anabolic function of miR-672-5p is mediated through Smurf1 suppression and Runx2 activation. Additionally, an absence of *in vitro* action of miR-672-5p was documented on osteoclastogenesis from bone marrow cell cultures[24] (Figures S2D–S2F).

miR-672-5p Treatment Mitigates Ovariectomy-Induced Sarcopenia

As it is reported that OVx rodents displayed a decrease in lean mass,[18] we next examined gastrocnemius muscle to investigate sarcopenia (muscle atrophy). At the end of 6-week treatment, body weight (Figure 5A) and lean mass (Figure 5B) were measured. To demonstrate sarcopenia in OVx animals, we estimated serum levels of creatine kinase, which is an indicator of skeletal muscle destruction. Serum levels of creatine kinase were higher in OVx mice compared with sham mice but were significantly lower in miR-672-5p mimic mice (Figure 5C). Histological analysis using H&E stain (Figure 5D) revealed a reduction in both cross-sectional area (Figure 5E) and Feret's diameter (Figure 5F) in OVx mice compared with sham, and miR-672-5p mimic significantly enhanced both parameters over OVx (Figures 5Eand 5F). Laminin, a protein of the extracellular matrix, is found in the basement membrane of muscle fibers, and a stable staining of laminin along the basement membrane is characteristic of healthy muscle fibers. Immunostaining with laminin antibody disclosed deterioration and shrinkage of muscle fibers in OVx animals, and miR-672-5p mimic not only enhanced muscle fibrillar architecture, as shown by the stable staining of laminin, but also enhanced muscle fiber size compared with OVx animals (Figure 5G). Evaluation of atrogin-1 expression was also done using immunohistochemistry and showed an enhanced staining in muscles of OVx mice, whereas miR-672-5p mimic displayed a reduction in its level (Figure 5H). Corroborating to sarcopenia in OVx animals, the expression of myogenic differentiation-1 (MyoD) was decreased compared with

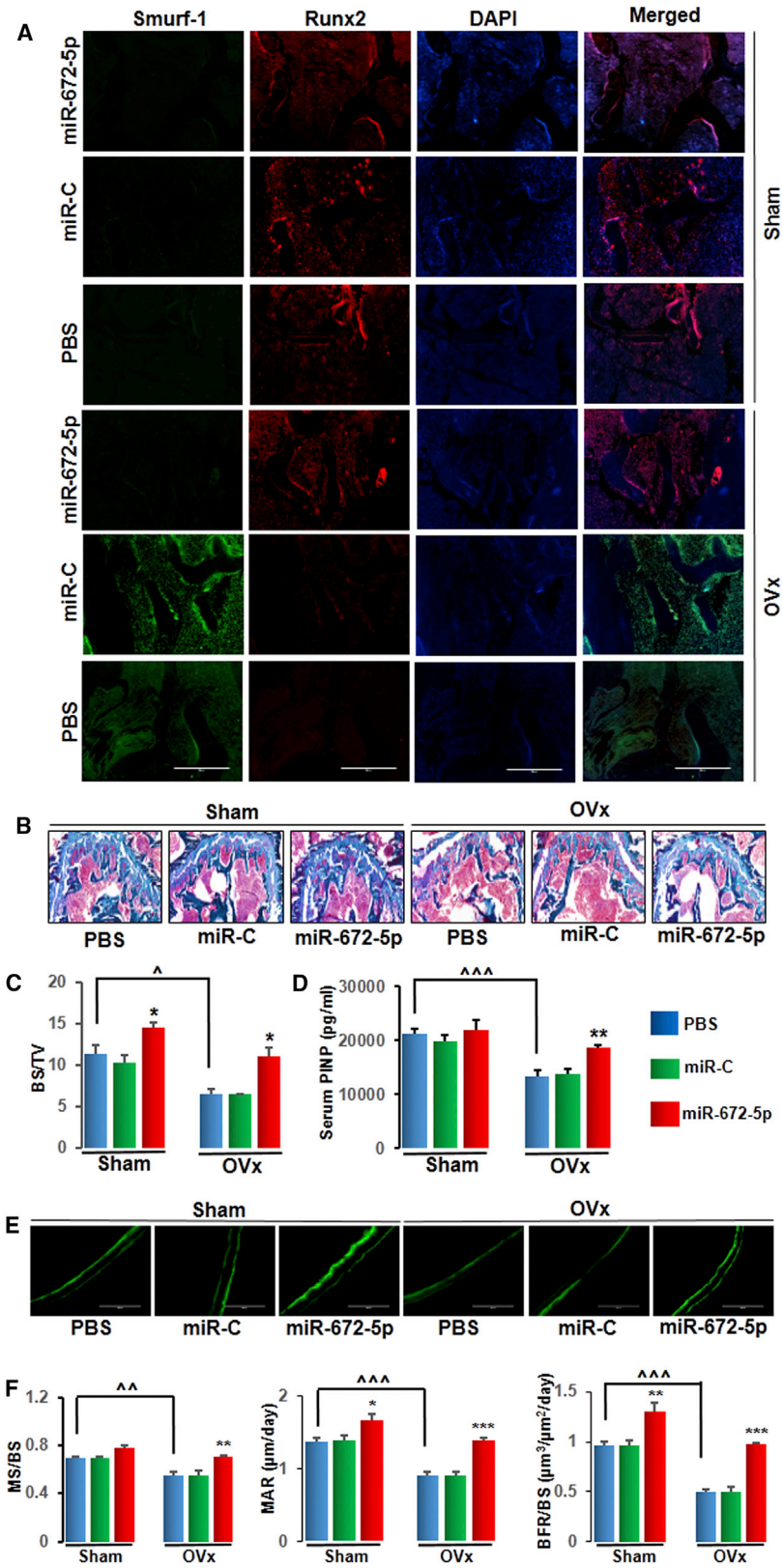

Figure 3. miR-672-5p Treatment Has an Anabolic Effect and Promotes Bone Formation

(A) Immunofluorescence assay in decalcified bone sections showed that miR-672-5p overexpression promoted Runx2 expression (red) and suppressed Smurf1 expression (green) as compared with the PBS-treated group (n = 3, magnification 20×). (B and C) Representative photomicrographs of Goldner's trichrome (GT) staining (B) of distal femurs from different groups and histomorphometric quantification; BS/TV (C) using the Bioquant software. Data are mean ± SE. *p < 0.05 compared with the PBS-treated group, or as shown ^p < 0.05; (n = 3, magnification 20×). (D) Osteogenic marker; serum P1NP concentration of different groups by ELISA. Data are mean ± SE. **p < 0.01 compared with the PBS-treated group, or as shown ^^^p < 0.001; (n = 6). (E) Representative photomicrographs of the calcein double labeling in the femur (n = 3, magnification 20×). (F) Quantification of data showing mineralizing surface normalized with bone surface (MS/BS), mineral apposition rate (MAR), and rate of bone formation, surface referent (BFR/BS). Data are mean ± SE. *p < 0.05, **p < 0.01 and ***p < 0.001 compared with the PBS-treated group, or as shown ^^p < 0.01 and ^^^p < 0.001. See also Figures S2A–S2C for histological examination of the femur metaphysis for osteoclast numbers and bone resorption surface estimates for *in vivo* experiments.

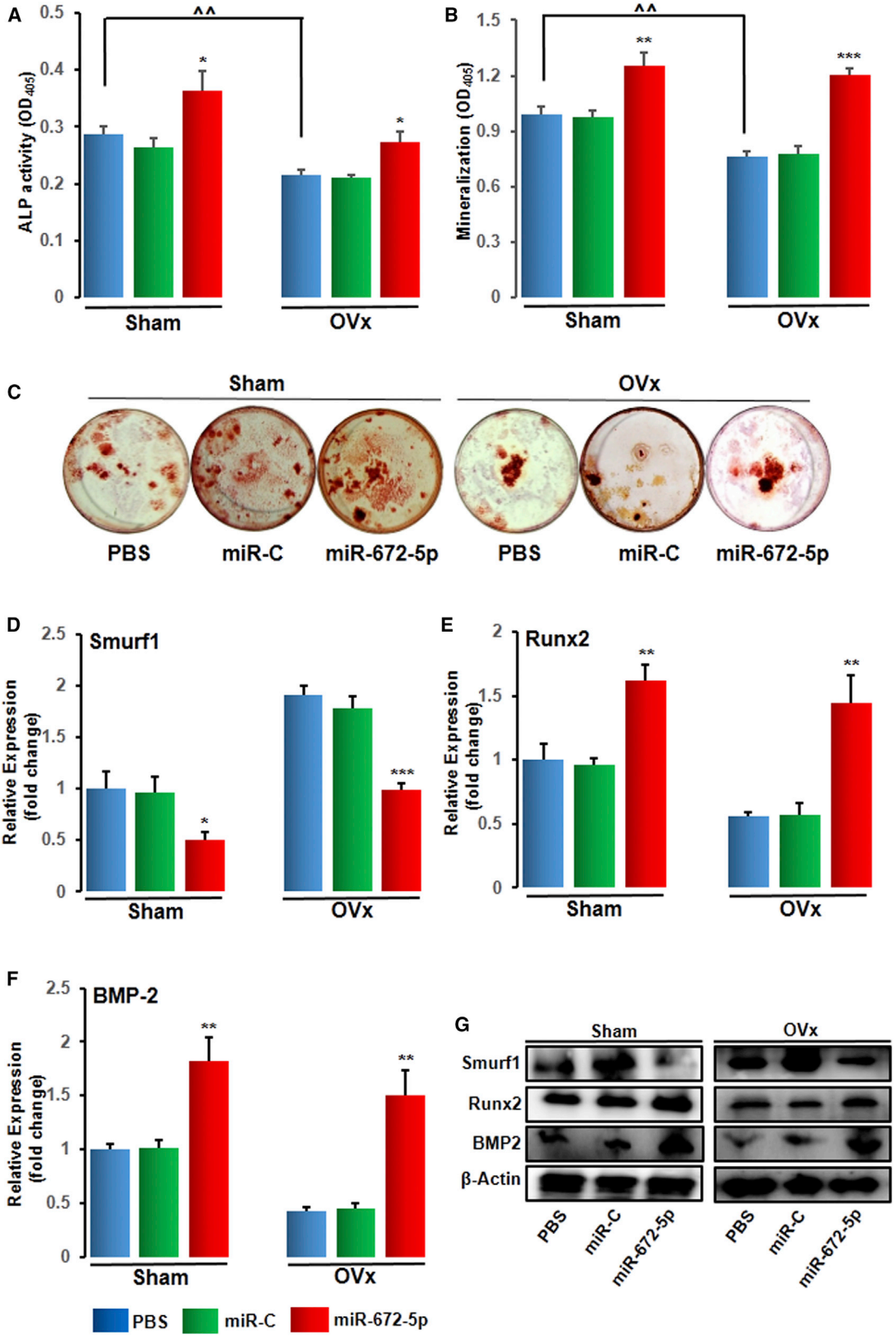

(legend on next page)

sham, and miR-672-5p mimic partly reversed the expression (Figure 5I). This data is consistent with previous reports.[18,25] Furthermore, augmented expression of muscle atrogenes, which stimulates protein catabolism and negatively affects muscular health. We noticed that there was an increase inatrogin-1 (Figure 5J) and Murf-1 (Figure 5K) in OVx mice compared with sham, and the expression of atrogenes was decreased in miR-672-5p mimic (Figure 5J and 5K). Expression of MyoD, atrogin-1, and Murf-1 was also assessed at the protein level (Figure 5L). These findings indicate that miR-672-5p overexpression reduces the atrophic characteristics of OVx mice.

DISCUSSION

We had recently identified potential miRNAs that regulate the lactation-to-weaning phase. Weaning phase is considered to be the anabolic window in terms of bone formation, as compared to lactation phase, where tremendous amount of bone is lost. miRNA profiling showed the differential expression of eight out of a total 4,716 detected miRNAs at the time of weaning, and the expression of five miRNAs (miR-672-5p, miR-874-3p, miR-451, miR-212, and miR-327) was increased, whereas three miRNAs (miR-204, miR-322-3p, and miR-664) were reduced.[12] This profiling urged that hitherto unacknowledged miRNAs were probably required in skeletogenesis during a physiologically critical reproductive window. Thus, we examined directly the effect of regulating the expression of one of these miRNAs, miR-672-5p, using particularly designed mimics and inhibitors. Of note is that a recent study reported that the expression of miRNA-672-5p is reduced in colon cancer with tumor progression,[26] and colorectal or colon cancer is related to muscle wasting and usually accompanied by bone loss.[27] Expression of miRNA-672 is also downregulated in X chromosome-linked muscular dystrophy (mdx) mice, a popular model for studying Duchenne muscular dystrophy.[28,29] These studies prompted us to study the effect of miR-672-5p in bone and the simultaneous effect on skeletal muscle. We noticed that miRNA-672-5p mimic transfection in osteoblast precursor cells promoted cell differentiation into a mature, mineralizing phenotype, and this was followed with enhanced expression of Runx2, BMP2, and Smad1, the osteogenic genes. Moreover, this effect was intervened through mimic-induced osteoblastogenesis and Runx2 expression; both were dependent on Smurf1 suppression. This is anticipated since there is previous confirmation for an interaction between miRNAs, Smurf1, and Runx2. For example, Runx2 can positively be modulated by miR-15b, which, in turn, inhibits Smurf1 to increase the expression of Runx2 and promotes osteoblast differentiation.[30] Similarly, we propound a pathway in which miR-672-5p decreases the expression of Smurf1 to increase Runx2 expression and osteoblast differentiation.

Of note is our result that expression of BMP2 is also modulated similarly, which is consistent with miR-15b-induced suppression of Smurf1, followed by enhancement of bone formation.[30] It is already known that BMP2 promotes Runx2 acetylation and inhibits Smurf1/2-mediated degradation of Runx2, whereas for the deacetylation of Runx2, Smurf1/2 permits the protein to face Smurf-mediated degradation.[30,31] Thus, we speculate that the inhibition of Smurf1 by miR-672-5p improves Runx2 acetylation, followed by BMP2-induced osteoblast differentiation.

The possible anabolic function of miR-672-5p was investigated in the *in vivo* system of 12-week-old female BALB/c mice in which the skeleton encountered active modeling. OVx or sham-operated mice were injected with either mimic (miR-672-5p), miR-C or PBS (as vehicle) intravenously through the tail vein, intermittently over 6 weeks. Mimic treatment inhibited loss of trabecular bone and enhanced bone strength in OVx mice as well as in the sham-operated mice. Notably, *ex vivo* cultures of osteoblast derived from BMCs from mimic-treated mice not only indicated confirmation of augmented osteoblastogenesis, mineralization, the formation of Cfu-ob, and the expression of BMP2 and Runx2, but also decreased Smurf1, necessarily corroborating our *in vitro* data. Thus, these results reveal a potential anabolic target for miR-672-5p. Since miR-672-5p is upregulated during weaning, it is plausible that it plays an important role in increasing skeletal mass following pregnancy and lactation.

The most recurrent metabolic abnormalities noticed after menopause include high fracture risk and muscle wasting.[32] In OVx mice with osteopenia, we demonstrated that miR-672-5p overexpression partly reversed trabecular bone mass, microarchitecture, and strength at femoral and vertebral column site, which represents the most prone sites for fractures in post-menopausal women. Longitudinal analysis using miR-672-5p mimic in osteopenic mice showed a gain of trabecular bone as well as partial restoration of OVx-induced sarcopenia, which are now progressively accepted as importantly modulating skeletal homeostasis.[33,34]

Post-menopausal women's lower lean body mass is correlated with high chances of hip fracture.[35] Because it has been reported that miRNA-672-5p is reduced with tumor progression in colon cancer, which is related to muscle wasting and usually accompanied by bone loss.[26,27] miRNA-672 is also downregulated in mdx mice, a

Figure 4. miR-672-5p Treatment Represses Smurf1 *In Vivo* to Promote Osteoblastogenesis

(A) ALP activity (OD, n = 6), (B) mineralization (OD, n = 6), and (C) representative wells of Cfu-ob formation. Data are mean ± SE. *p < 0.05, **p < 0.01, and ***p < 0.001 compared with the PBS-treated group, or as shown ^^p < 0.01. mRNA expression (qPCR, in triplicate) of Smurf1 (D), Runx2 (E), and BMP2 (F) and protein expression (G) (western blotting) of Smurf1 (ab38866-Abcam; 1:1,000), Runx2 (ab76956-Abcam; 1:1,000), and BMP2 (ab14933-Abcam; 1:1,000) in osteoblasts from sham-operated (Sham) or ovariectomized (OVx) mice that were given PBS (0.2 mL), scrambled miR (miR-C, 7.0 mg kg^{-1}), or miR-672-5p (7.0 mg kg^{-1}). β-actin (sc-47778 Santa Cruz Biotechnology; 1:500) was taken as loading control. Secondary antibodies (either anti-rabbit or anti-mouse; 1:10,000) were HRP conjugated (Sigma-Aldrich). Data are mean ± SE. *p < 0.05, **p < 0.01, and ***p < 0.001 compared with the PBS-treated group. See also Figures S2D–S2F for *in vitro* actions of microRNA-672-5p on osteoclastogenesis from bone marrow cell cultures.

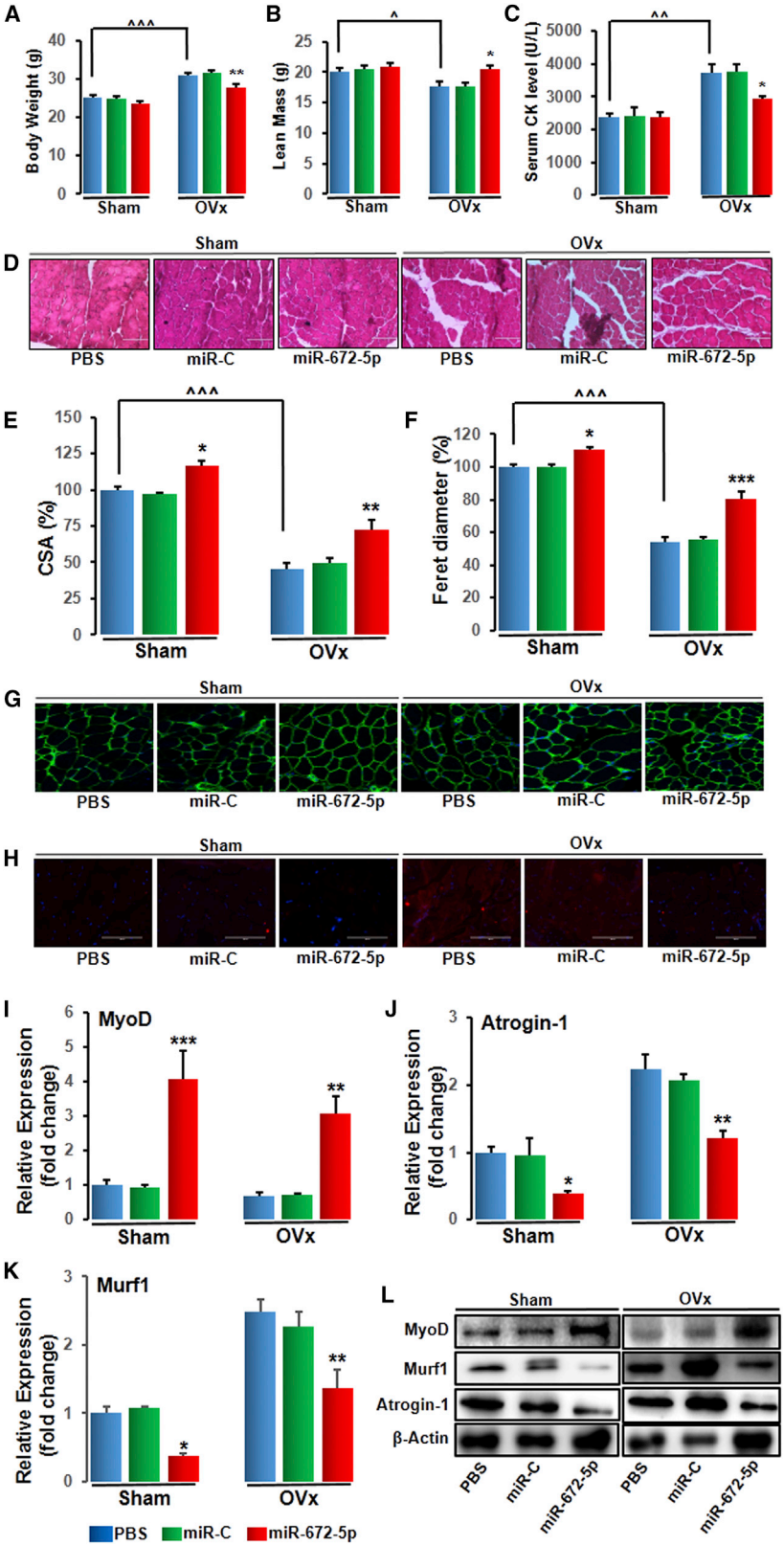

Figure 5. miR-672-5p Treatment Mitigates Ovariectomy-Induced Sarcopenia

(A) Body weight, (B) lean mass, and (C) serum CK levels. Data are mean ± SE. *p < 0.05 and **p < 0.01 compared with the PBS-treated group, or as shown ^p < 0.05, ^^p < 0.01, and ^^^p < 0.001 (n ≥ 6 mice per group). (D) Representative photomicrographs of H&E-stained sections of gastrocnemius muscle from the indicated groups (n = 3, magnification 40×). (E) Cross-sectional area (CSA) and (F) Feret's diameter. Data are mean ± SE. *p < 0.05, **p < 0.01, and ***p < 0.001 compared with the PBS-treated group, or as shown ^^^p < 0.001. (G and H) Immunostaining for laminin (G) and immunostaining for Atrogin-1 (H) (n = 3, magnification 40×). mRNA expression (qPCR, in triplicate) of MyoD (I), Atrogin-1 (J), and MuRF-1 (K) and protein expression (L) (western blotting) of muscle differentiation marker; MyoD (MA1-41017-Thermo Scientific; 1:1,000), catabolic markers, atrogin-1 (ab74023-Abcam; 1:1,000), and muscle ring-finger protein-1 (MuRF-1, ab183094-Abcam; 1:1,000) from gastrocnemius muscles of indicated groups. β-actin (sc-47778 Santa Cruz Biotechnology; 1:500) was taken as a loading control. Secondary antibodies (either anti-rabbit or anti-mouse; 1:10,000) were HRP conjugated (Sigma-Aldrich). Data are mean ± SE. *p < 0.05, **p < 0.01, and ***p < 0.001 compared with the PBS-treated group.

popular model for studying Duchenne muscular dystrophy.[28,29] In agreement with previous reports, we thought that muscle mass restoration in OVx mice by miR-672-5p could be a result of alleviating OVx-induced muscle atrophy. miR-672-5p attenuated OVx-induced destruction in myofibrillar architecture and abrogated changes in atrogenes and anti-atrophy factors, and the possible mechanism arose in the restoration of OVx-induced downregulation in muscle miR-672 expression. In conclusive summary, data suggest that miR-672-5p could restore both osteopenia and sarcopenia in a pre-clinical setup of post-menopausal osteoporosis and also suggest a pharmacologic option for the treatment of osteopenia and/or sarcopenia in post-menopausal condition. It is clear that protecting bone mass promotes survival in sarcopenia. Future studies are needed to determine whether strategies aimed at promoting bone formation can also improve outcomes and survival in sarcopenia.

MATERIALS AND METHODS

Chemicals and Reagents

The miRVana miRNA isolation kit, miR-672-5p mimic, and inhibitor were bought from Ambion (Life Technologies, USA) and BMP2 and P1NP ELISA from R&D Systems (Minneapolis, MN) and Elabscience (Houston, TX), respectively. Serum CK activity assay kit was from Abcam (Cambridge, UK). qPCRs were executed with the help of StepOne real-time PCR system and a TaqMan 5′ nuclease probe method (Applied Biosystems), and U6 was used to normalize miRNA transcripts.[31,36,37]

Calvarial Cell Culture

For *in vitro* studies, about 5–10 calvaria were collected from 1- to 2-day-old BALB/c mouse pups. In brief, the individual calvarium was surgically separated from the skull. Sutures were separated, and adherent soft tissue material was removed by gentle scraping. Isolated calvariae were pooled and kept for repeated digestion (15 min/digestion) with 0.1% dispase and 0.1% collagenase P enzymes, which were used to release the cells. The supernatant collected from the first digestion was discarded, and then cells from the next three to four digestions were pooled and cultured in α-MEM (α modified essential medium) supplemented with 10% fetal calf serum (FCS) and 1% penicillin-streptomycin at 37°C in a humidified atmosphere of 5% CO_2 and 95% air. Calvarial cells were permitted to grow 70%–80% confluence for the experiments.[38]

ALP and Mineralization Assay of BMCs

After the treatment periods, BMCs from the long bones of mice were collected in osteoblast differentiation medium containing 10^{-7} M dexamethasone. BMC culture was continued for 21 days, and the medium was refreshed once every 48 h. At the end of the BMC culture, ALP activity was estimated at 405 nm, and alizarin Red-S was used to stain mineralized nodules and quantified at 405 nm.[38]

Analysis of miRNA Target Site Prediction

In silico screening studies of the putative targets were carried out for miRNA-672-5p using TargetScan and miRBase bioinformatics tools by searching for the presence of sites that match the seed region of miRNA.[39,40]

Transfection in Osteoblast Cells

Transfection studies with miRNA-672-5p mimic and inhibitor or siRNA were done into mouse calvarial osteoblast cells at 50%–60% confluence with reduced-serum and antibiotic-free OptiMEM with the help of transfection agent Lipofectamine (Invitrogen). ALP activity, mineralization assay, and qPCR analysis were executed following protocols published previously.[41,42] The sequences of primer sets used in this study are shown in the Supplemental Information (Table S1). Western blotting utilized an enhanced chemiluminescence system (GE Healthcare) according to the manufacturer's instructions.[31] For the luciferase reporter assay, pEZX-MT06 vector (wild-type 3′ UTR of Smurf-1, catalog no. MmiT036100-MT06, GeneCopoeia) was co-transfected into osteoblasts. In addition, Runx2-Luc and Renilla luciferase vectors (catalog no. MPRM13038, GeneCopoeia) were also co-transfected for Runx2 reporter promoter assay, and luciferase activity was measured using a dual-assay luciferase kit.[41] Please see the Supplemental Materials and Methods for *in vitro* actions of miRNA-672-5p on osteoclastogenesis from bone marrow cell cultures.

In Vivo Studies

All animal care and experimental procedures were approved by the Institutional Animal Ethics Committee (IAEC) (approval no. IAEC/2017/F-235) and the Council of Scientific and Industrial Research-Central Drug Research Institute (CSIR-CDRI) and executed according to the regulations of the Council for the Purpose of Control and Supervision of Experiments on Animals, Ministry of Social Justice and Empowerment, Government of India. Female BALB/c mice (weighing 22 ± 2 g each) were housed in a 12-h/12-h light/dark cycle with controlled temperature (22°C–24°C) and humidity (50%–60%).[41] Standard rodent chow diet and water were provided *ad libitum*.[41] *In vivo* mimic of miRNA-672-5p, miR-C (control miRNA), or a comparable volume of PBS (0.2 mL, as vehicle) were administered intravenously through tail vein with the help of an anionic liposome (Invivofectamine 3.0, Life Technologies), which enables the fusion of the liposome-nucleic acid complex with the cell membrane and subsequent uptake by endocytosis.[12] μCT analysis was performed using a SkyScan 1076 CT scanner (Aartselaar, Antwerp, Belgium). In brief, long bones (femora and tibiae) and vertebrae were scanned at a nominal resolution of 18 mm. One hundred projections at an angular range of 180° were obtained, and reconstruction of the image slices was done using a modified Feldkamp algorithm (according to Sky Scan Nrecon software). μCT parameters, including BV/TV (%),Tb.Sp (mm), Tb.N (mm^{-1}), Tb.Pf (mm^{-1}), SMI, and Conn.Dn, mm^{-3} were calculated. vBMD analysis of the femur, tibia, and vertebrae was done using μCT by following the previously published protocols.[43] For bone biomechanical analysis, femora and vertebrae of different groups were used in three-point bending and compression test, respectively, using a bone-strength tester (model TK-252C; Muromachi Kikai, Tokyo Japan).[41,42] Values of power, strength, and stiffness were calculated to check bone biomechanical

properties. In addition, analysis of qPCR and western blotting for bone and muscle tissues was done as described above.[31,41,42] To assess lean mass, mice were scanned using EchoMRI-500 (EchoMRI, Singapore) according to manufacturer's protocol.[18]

Bone Histomorphometry

Bone formation was evaluated with double fluorochrome labeling by injecting calcein (5 mg/kg) on the 15th day of the treatment and second days before autopsy into all groups of mice. MS/BS, MAR, and BFR/BS in femur (undecalcified section of 50 μm) was determined with the help of fluorescence imaging and Leica-Qwin software (Leica Microsystems, Buffalo Grove, IL).[12,44] To assess BS/TV (ratio of the segmented bone surface to the total volume of the region of interest), undecalcified sections (5 μm) were obtained from femur bones embedded in polymerized methyl methacrylate and stained with GT.[44,45] BS/TV (mm^2/mm^3) was assessed using Bioquant Osteo Software (Bioquant Image Analysis, Nashville, TN, USA). Please see the Supplemental Materials and Methods for histological examination of the femur for osteoclast numbers and bone resorption surface estimates for *in vivo* experiments.

Immunohistochemistry of Bone

Immunohistochemistry was done to check the expression level of Smurf11 and Runx2 in the trabecular region (decalcified section; 5 μm) of distal femur metaphysis. Femur bones were fixed in 4% paraformaldehyde in 0.1 M PBS (pH 7.4) and decalcified by immersion in decalcifying solution lite (Sigma-Aldrich, St. Louis, MO, USA) for 1 week and embedded in paraffin. Longitudinal bone sections were then blocked by 5% goat serum for 1 h at room temperature and incubated overnight with the primary antibodies (Smurf1, ab38866-Abcam, 1:100 dilution; Runx2, ab76956-Abcam, 1:100 dilution). Sections were then incubated with Alexa Flour 488 (Invitrogen, USA) and Cy3 (Sigma-Aldrich, USA) secondary antibodies in 1:200 dilution for 1 h at room temperature. Sections were washed with PBS and mounted with ProLong Gold Antifade Mountant with DAPI (Life Technologies, USA). Fluorescence was captured using a fluorescent microscope (Eclipse 80i, Nikon, Tokyo, Japan) with the aid of appropriate filter.[46]

Histology and Immunostaining of Muscle Tissue

Study of histological and immunofluorescence analysis of muscle tissues was performed as detailed previously.[47] In brief, gastrocnemius muscles were collected and kept for 4 to 8 h in chilled PBS, followed by the transfer of the tissues in 30% sucrose PBS solution at 4°C till they reached to the bottom. Then, muscle tissues were embedded in optimal cutting temperature (OCT) tissue-freezing medium, followed by cryosectioning at −21°C using a Cryotome FSE Cryostat (Thermo Scientific). 7-μm-thick tissue sections were obtained on poly-L-lysine-coated slides, air-dried at room temperature, and used for H&E staining and immunostaining. For H&E staining, rehydration of sections was done in PBS for 10 min, followed by fixing in 10% formalin for 3 min, and staining of sections was done with H&E, followed by mounting of slides with distyrene, plasticizer, and xylene (DPX). Stained sections then were examined under a microscope. Cross-sectional area and Feret's diameter of the muscle tissues were quantitated using ImageJ software (NIH, USA). For immunostaining of muscle tissue, in brief, cryosections were fixed with 4% paraformaldehyde in cold PBS and permeabilized with 0.5% Triton X-100 for 20 min at room temperature. Sections were washed with PBS and then blocked with 10% BSA for 30 min, followed by incubation with primary antibodies (Atrogin-1, ab74023-Abcam, 1:100 dilution; Laminin, ab11575-Abcam, 1:100 dilution) for overnight at 4°C. Sections were, the next day, washed with PBS and incubated with Alexa Flour 488 (Invitrogen, USA) and Cy3 (Sigma, USA) secondary antibodies in 1:200 dilution at room temperature for 1 h. Slides were mounted with antifade DAPI using coverslips. Sections were then examined using a fluorescence microscope (Eclipse 80i, Nikon Corporation, Tokyo, Japan).

Biochemical Assays

N-terminal type 1 procollagen (P1NP) levels[18] and creatine kinase (CK) activity[48] in serum were measured using P1NP ELISA kit (Elabscience, Houston, TX) and CK activity assay kit (Abcam, Cambridge, UK) following manufacturer's protocol. In addition, levels of BMP2 were also checked in conditioned media collected during transfection studies with miRNA-672-5p following manufacturer's protocol.[12]

Statistical Analysis

One-way ANOVA was applied for experiments with multiple comparisons followed by Newman-Keuls test of significance with the help of GraphPad Prism v.5. Student's t test was employed for experiments with only two treatments.

SUPPLEMENTAL INFORMATION

Supplemental Information includes two figures, one table, and Supplemental Materials and Methods and can be found with this article online at https://doi.org/10.1016/j.omtn.2019.01.002.

AUTHOR CONTRIBUTIONS

R.T. and N.A. conceptualized the study and designed experiments. N.A., P. Kushwaha, A.K., A.K.T., P. Kothari, S.A., V.K., and V.K.M. performed experiments. R.T. supervised experiments. All authors analyzed data and contributed to the discussion. R.T. and N.A. wrote the paper.

CONFLICTS OF INTEREST

The authors declare no conflict of interest.

ACKNOWLEDGMENTS

R.T. acknowledges funding from the Department of Biotechnology (DBT), New Delhi, India (GAP0127), and the Council of Scientific and Industrial Research (CSIR), New Delhi, India (BSC0201 and BSC0111). The authors acknowledge Dr. Kavita Singh and Dr. Kalyan Mitra of the Sophisticated Analytical Instrument Facility (SAIF) unit of CSIR-Central Drug Research Institute (CDRI) for facilitating confocal microscopy. N.A. acknowledges fellowship from CSIR Direct SRF (31/4(1207)/2015-EMR-I). P. Kushwaha, A.K., and

A.K.T. acknowledge fellowships from CSIR; P. Kothari, S.A., and V.K. acknowledge fellowships from the University Grants Commission (UGC); and V.K.M. acknowledges a National Post-Doctoral Fellowship (PDF/2015/000915) from the Science and Engineering Research Board (SERB), New Delhi, India.

REFERENCES

1. Reginster, J.Y., Beaudart, C., Buckinx, F., and Bruyère, O. (2016). Osteoporosis and sarcopenia: two diseases or one? Curr. Opin. Clin. Nutr. Metab. Care *19*, 31–36.
2. Levine, M.E., Lu, A.T., Chen, B.H., Hernandez, D.G., Singleton, A.B., Ferrucci, L., Bandinelli, S., Salfati, E., Manson, J.E., Quach, A., et al. (2016). Menopause accelerates biological aging. Proc. Natl. Acad. Sci. USA *113*, 9327–9332.
3. Di Monaco, M., Castiglioni, C., De Toma, E., Gardin, L., Giordano, S., Di Monaco, R., and Tappero, R. (2015). Presarcopenia and sarcopenia in hip-fracture women: prevalence and association with ability to function in activities of daily living. Aging Clin. Exp. Res. *27*, 465–472.
4. Kim, S., Won, C.W., Kim, B.S., Choi, H.R., and Moon, M.Y. (2014). The association between the low muscle mass and osteoporosis in elderly Korean people. J. Korean Med. Sci. *29*, 995–1000.
5. Kohrt, W.M., Barry, D.W., and Schwartz, R.S. (2009). Muscle forces or gravity: what predominates mechanical loading on bone? Med. Sci. Sports Exerc. *41*, 2050–2055.
6. Girgis, C.M., Mokbel, N., and Digirolamo, D.J. (2014). Therapies for musculoskeletal disease: can we treat two birds with one stone? Curr. Osteoporos. Rep. *12*, 142–153.
7. Chen, J., Qiu, M., Dou, C., Cao, Z., and Dong, S. (2015). MicroRNAs in Bone Balance and Osteoporosis. Drug Dev. Res. *76*, 235–245.
8. Pi, C., Li, Y.P., Zhou, X., and Gao, B. (2015). The expression and function of microRNAs in bone homeostasis. Front. Biosci. *20*, 119–138.
9. Tang, P., Xiong, Q., Ge, W., and Zhang, L. (2014). The role of microRNAs in osteoclasts and osteoporosis. RNA Biol. *11*, 1355–1363.
10. Eguchi, T., Watanabe, K., Hara, E.S., Ono, M., Kuboki, T., and Calderwood, S.K. (2013). OstemiR: a novel panel of microRNA biomarkers in osteoblastic and osteocytic differentiation from mesencymal stem cells. PLoS ONE *8*, e58796.
11. Lian, J.B., Stein, G.S., van Wijnen, A.J., Stein, J.L., Hassan, M.Q., Gaur, T., and Zhang, Y. (2012). MicroRNA control of bone formation and homeostasis. Nat. Rev. Endocrinol. *8*, 212–227.
12. Kushwaha, P., Khedgikar, V., Sharma, D., Yuen, T., Gautam, J., Ahmad, N., Karvande, A., Mishra, P.R., Trivedi, P.K., Sun, L., et al. (2016). MicroRNA 874-3p Exerts Skeletal Anabolic Effects Epigenetically during Weaning by Suppressing Hdac1 Expression. J. Biol. Chem. *291*, 3959–3966.
13. Lebel, E., Mishukov, Y., Babchenko, L., Samueloff, A., Zimran, A., and Elstein, D. (2014). Bone mineral density in gravida: effect of pregnancies and breast-feeding in women of differing ages and parity. J. Osteoporos. *2014*, 897182.
14. Bolzetta, F., Veronese, N., De Rui, M., Berton, L., Carraro, S., Pizzato, S., Girotti, G., De Ronch, I., Manzato, E., Coin, A., and Sergi, G. (2014). Duration of breastfeeding as a risk factor for vertebral fractures. Bone *68*, 41–45.
15. Miller, S.C., and Bowman, B.M. (1998). Comparison of bone loss during normal lactation with estrogen deficiency osteopenia and immobilization osteopenia in the rat. Anat. Rec. *251*, 265–274.
16. Ardeshirpour, L., Dann, P., Adams, D.J., Nelson, T., VanHouten, J., Horowitz, M.C., and Wysolmerski, J.J. (2007). Weaning triggers a decrease in receptor activator of nuclear factor-kappaB ligand expression, widespread osteoclast apoptosis, and rapid recovery of bone mass after lactation in mice. Endocrinology *148*, 3875–3886.
17. Liu, X.S., Ardeshirpour, L., VanHouten, J.N., Shane, E., and Wysolmerski, J.J. (2012). Site-specific changes in bone microarchitecture, mineralization, and stiffness during lactation and after weaning in mice. J. Bone Miner. Res. *27*, 865–875.
18. China, S.P., Pal, S., Chattopadhyay, S., Porwal, K., Kushwaha, S., Bhattacharyya, S., Mittal, M., Gurjar, A.A., Barbhuyan, T., Singh, A.K., et al. (2017). Globular adiponectin reverses osteo-sarcopenia and altered body composition in ovariectomized rats. Bone *105*, 75–86.
19. Zhao, M., Qiao, M., Harris, S.E., Oyajobi, B.O., Mundy, G.R., and Chen, D. (2004). Smurf1 inhibits osteoblast differentiation and bone formation in vitro and in vivo. J. Biol. Chem. *279*, 12854–12859.
20. Yamashita, M., Ying, S.X., Zhang, G.M., Li, C., Cheng, S.Y., Deng, C.X., and Zhang, Y.E. (2005). Ubiquitin ligase Smurf1 controls osteoblast activity and bone homeostasis by targeting MEKK2 for degradation. Cell *121*, 101–113.
21. Shimazu, J., Wei, J., and Karsenty, G. (2016). Smurf1 Inhibits Osteoblast Differentiation, Bone Formation, and Glucose Homeostasis through Serine 148. Cell Rep. *15*, 27–35.
22. Wang, C., Xiao, F., Qu, X., Zhai, Z., Hu, G., Chen, X., and Zhang, X. (2017). Sitagliptin, An Anti-diabetic Drug, Suppresses Estrogen Deficiency-Induced Osteoporosis*In Vivo* and Inhibits RANKL-Induced Osteoclast Formation and Bone Resorption *In Vitro*. Front. Pharmacol. *8*, 407.
23. Guo, R., Yamashita, M., Zhang, Q., Zhou, Q., Chen, D., Reynolds, D.G., Awad, H.A., Yanoso, L., Zhao, L., Schwarz, E.M., et al. (2008). Ubiquitin ligase Smurf1 mediates tumor necrosis factor-induced systemic bone loss by promoting proteasomal degradation of bone morphogenetic signaling proteins. J. Biol. Chem. *283*, 23084–23092.
24. Kaneki, H., Guo, R., Chen, D., Yao, Z., Schwarz, E.M., Zhang, Y.E., Boyce, B.F., and Xing, L. (2006). Tumor necrosis factor promotes Runx2 degradation through up-regulation of Smurf1 and Smurf2 in osteoblasts. J. Biol. Chem. *281*, 4326–4333.
25. Khan, M.P., Singh, A.K., Joharapurkar, A.A., Yadav, M., Shree, S., Kumar, H., Gurjar, A., Mishra, J.S., Tiwari, M.C., Nagar, G.K., et al. (2017). Erratum. Pathophysiological Mechanism of Bone Loss in Type 2 Diabetes Involves Inverse Regulation of Osteoblast Function by PGC-1α and Skeletal Muscle Atrogenes: AdipoR1 as a Potential Target for Reversing Diabetes-Induced Osteopenia. Diabetes 2015;64:2609-2623. Diabetes *66*, 3142–3143.
26. Teng, Y., Ren, Y., Hu, X., Mu, J., Samykutty, A., Zhuang, X., Deng, Z., Kumar, A., Zhang, L., Merchant, M.L., et al. (2017). MVP-mediated exosomal sorting of miR-193a promotes colon cancer progression. Nat. Commun. *8*, 14448.
27. Bonetto, A., Kays, J.K., Parker, V.A., Matthews, R.R., Barreto, R., Puppa, M.J., Kang, K.S., Carson, J.A., Guise, T.A., Mohammad, K.S., et al. (2017). Differential Bone Loss in Mouse Models of Colon Cancer Cachexia. Front. Physiol. *7*, 679.
28. Falcone, G., Perfetti, A., Cardinali, B., and Martelli, F. (2014). Noncoding RNAs: emerging players in muscular dystrophies. BioMed Res. Int. *2014*, 503634.
29. Vignier, N., Amor, F., Fogel, P., Duvallet, A., Poupiot, J., Charrier, S., Arock, M., Montus, M., Nelson, I., Richard, I., et al. (2013). Distinctive serum miRNA profile in mouse models of striated muscular pathologies. PLoS ONE *8*, e55281.
30. Vimalraj, S., Partridge, N.C., and Selvamurugan, N. (2014). A positive role of microRNA-15b on regulation of osteoblast differentiation. J. Cell. Physiol. *229*, 1236–1244.
31. Khedgikar, V., Kushwaha, P., Gautam, J., Verma, A., Changkija, B., Kumar, A., Sharma, S., Nagar, G.K., Singh, D., Trivedi, P.K., et al. (2013). Withaferin A: a proteasomal inhibitor promotes healing after injury and exerts anabolic effect on osteoporotic bone. Cell Death Dis. *4*, e778.
32. Hida, T., Harada, A., Imagama, S., and Ishiguro, N. (2013). Managing sarcopenia and its related-fractures to improve quality of life in geriatric populations. Aging Dis. *5*, 226–237.
33. Ormsbee, M.J., Prado, C.M., Ilich, J.Z., Purcell, S., Siervo, M., Folsom, A., and Panton, L. (2014). Osteosarcopenic obesity: the role of bone, muscle, and fat on health. J. Cachexia Sarcopenia Muscle *5*, 183–192.
34. Lecka-Czernik, B., and Rosen, C.J. (2015). Energy Excess, Glucose Utilization, and Skeletal Remodeling: New Insights. J. Bone Miner. Res. *30*, 1356–1361.
35. Capozza, R.F., Cure-Cure, C., Cointry, G.R., Meta, M., Cure, P., Rittweger, J., and Ferretti, J.L. (2008). Association between low lean body mass and osteoporotic fractures after menopause. Menopause *15*, 905–913.
36. Gámez, B., Rodríguez-Carballo, E., Bartrons, R., Rosa, J.L., and Ventura, F. (2013). MicroRNA-322 (miR-322) and its target protein Tob2 modulate Osterix (Osx) mRNA stability. J. Biol. Chem. *288*, 14264–14275.
37. Kureel, J., Dixit, M., Tyagi, A.M., Mansoori, M.N., Srivastava, K., Raghuvanshi, A., Maurya, R., Trivedi, R., Goel, A., and Singh, D. (2014). miR-542-3p suppresses osteoblast cell proliferation and differentiation, targets BMP-7 signaling and inhibits bone formation. Cell Death Dis. *5*, e1050.

38. Kushwaha, P., Khedgikar, V., Gautam, J., Dixit, P., Chillara, R., Verma, A., Thakur, R., Mishra, D.P., Singh, D., Maurya, R., et al. (2014). A novel therapeutic approach with Caviunin-based isoflavonoid that en routes bone marrow cells to bone formation via BMP2/Wnt-β-catenin signaling. Cell Death Dis. *5*, e1422.

39. Grimson, A., Farh, K.K., Johnston, W.K., Garrett-Engele, P., Lim, L.P., and Bartel, D.P. (2007). MicroRNA targeting specificity in mammals: determinants beyond seed pairing. Mol. Cell *27*, 91–105.

40. John, B., Enright, A.J., Aravin, A., Tuschl, T., Sander, C., and Marks, D.S. (2004). Human MicroRNA targets. PLoS Biol. *2*, e363.

41. Gautam, J., Choudhary, D., Khedgikar, V., Kushwaha, P., Singh, R.S., Singh, D., Tiwari, S., and Trivedi, R. (2014). Micro-architectural changes in cancellous bone differ in female and male C57BL/6 mice with high-fat diet-induced low bone mineral density. Br. J. Nutr. *111*, 1811–1821.

42. Sashidhara, K.V., Kumar, M., Khedgikar, V., Kushwaha, P., Modukuri, R.K., Kumar, A., Gautam, J., Singh, D., Sridhar, B., and Trivedi, R. (2013). Discovery of coumarin-dihydropyridine hybrids as bone anabolic agents. J. Med. Chem. *56*, 109–122.

43. Bouxsein, M.L., Boyd, S.K., Christiansen, B.A., Guldberg, R.E., Jepsen, K.J., and Müller, R. (2010). Guidelines for assessment of bone microstructure in rodents using micro-computed tomography. J. Bone Miner. Res. *25*, 1468–1486.

44. Khan, M.P., Khan, K., Yadav, P.S., Singh, A.K., Nag, A., Prasahar, P., Mittal, M., China, S.P., Tewari, M.C., Nagar, G.K., et al. (2016). BMP signaling is required for adult skeletal homeostasis and mediates bone anabolic action of parathyroid hormone. Bone *92*, 132–144.

45. Goldner, J. (1938). A modification of the masson trichrome technique for routine laboratory purposes. Am. J. Pathol. *14*, 237–243.

46. Li, S.F., Tang, J.J., Chen, J., Zhang, P., Wang, T., Chen, T.Y., Yan, B., Huang, B., Wang, L., Huang, M.J., et al. (2015). Regulation of bone formation by baicalein via the mTORC1 pathway. Drug Des. Devel. Ther. *9*, 5169–5183.

47. Singh, A.K., Shree, S., Chattopadhyay, S., Kumar, S., Gurjar, A., Kushwaha, S., Kumar, H., Trivedi, A.K., Chattopadhyay, N., Maurya, R., et al. (2017). Small molecule adiponectin receptor agonist GTDF protects against skeletal muscle atrophy. Mol. Cell. Endocrinol. *439*, 273–285.

48. Velders, M., Schleipen, B., Fritzemeier, K.H., Zierau, O., and Diel, P. (2012). Selective estrogen receptor-β activation stimulates skeletal muscle growth and regeneration. FASEB J. *26*, 1909–1920.